12-15-2011

Fragile Binary Candidates in the SDSS DR8 Spectroscopic Archive

J. K. Zhao
Florida Institute of Technology

Terry D. Oswalt
Florida Institute of Technology, oswaltt1@erau.edu

G. Zhao
Chinese Academy of Sciences

Scholarly Commons Citation
Zhao, J., Oswalt, T. D., & Zhao, G. (2011). Fragile Binary Candidates in the SDSS DR8 Spectroscopic Archive. *The Astronomical Journal, 143*(2). https://doi.org/10.1088/0004-6256/143/2/31

The Astronomical Journal, 143:31 (11pp), 2012 February doi:10.1088/0004-6256/143/2/31

FRAGILE BINARY CANDIDATES IN THE SDSS DR8 SPECTROSCOPIC ARCHIVE

J. K. Zhao[1,2], T. D. Oswalt[1], and G. Zhao[2]
[1] Florida Institute of Technology, Melbourne, FL 32901, USA; jzhao@fit.edu, toswalt@fit.edu
[2] Key Laboratory of Optical Astronomy, National Astronomical Observatories, Chinese Academy of Sciences, Beijing 100012, China; gzhao@bao.ac.cn
Received 2011 August 23; accepted 2011 November 7; published 2011 December 15

ABSTRACT

We present a catalog of 80 very wide fragile binary candidates (projected separations >10,000 AU) from the Sloan Digital Sky Survey Data Release Eight spectral archive. The pairs were selected based on proper motion, radial velocity, metallicity, and photometric parallax criteria. The angular separations of these pairs range from 3″ to 250″. The peak in the metallicity distribution of these pairs is about −0.5 dex of solar metallicity. Space motions and reduced proper motion diagrams indicate that all these pairs are members of the disk. The chromospheric activity index $S_{\rm HK}$ of each component in 38 binary candidates having spectra of high signal-to-noise ratio and member stars of three open clusters (NGC 2420, M67, and NGC 6791) were measured. The $S_{\rm HK}$ versus color relation for these binary candidates is consistent with the trend seen in these open clusters. The ages implied by this relation suggest that fragile wide pairs can survive longer than 8 Gyr.

Key words: stars: activity – stars: chromospheres

1. INTRODUCTION

Wide fragile binaries by definition have large semimajor axes ($a \geqslant 100$ AU). Thus, each component may be assumed to have evolved independently, unaffected by mass exchange or tidal coupling that complicate the evolution of closer pairs (Greenstein 1986). It may also be assumed that members of such binaries are coeval. Essentially, each may be regarded as an open cluster with only two components. Fragile binaries are important probes of the nature of halo dark matter, the evolution of the stellar halo, and the metallicities, masses, and ages of field stars (see Chanamé 2007). To better understand the formation (Kouwenhoven et al. 2010) and evolution (Jiang & Tremaine 2010) of wide binaries, large samples are needed.

At present, candidate fragile binaries have been selected mainly by searching for common proper motion (CPM) pairs. Luyten (1979, 1988) pioneered this technique using Schmidt telescope plates and a blink microscope. He detected more than 6000 wide pairs with $|\mu| > 100$ mas yr^{-1}. This method has since been used to find fragile binaries in the AGK 3 stars by Halbwachs (1986), in the revised New Luyten Two-tenths catalog (Salim & Gould 2003) by Chanamé & Gould (2004), and among the *Hipparcos* stars in the Lepine–Shara Proper Motion-North catalog (Lépine & Shara 2005; Lépine & Bongiorno 2007). All of these studies used magnitude-limited high proper motion catalogs and thus are limited mostly to nearby stars.

Recent large-scale surveys such as the Sloan Digital Sky Survey (SDSS; York et al. 2000), the Two Micron All Sky Survey (Cutri et al. 2003), and the UKIRT Infrared Deep Sky Survey (Lawrence et al. 2007) have yielded samples with good photometric data that are useful in selecting more distant fragile binaries when combined with proper motion information. Sesar et al. (2008) searched the SDSS Data Release Six (DR6; Adelman-McCarthy et al. 2008) for fragile binaries with angular separations up to 30″ using a novel statistical technique that minimizes the difference between the distance moduli obtained from photometric parallax relations for candidate pairs. They matched proper motion components to within 5 mas yr^{-1} with absolute proper motions of 15–400 mas yr^{-1}. Their search identified ∼14,000 total candidates with excellent completeness. However, one third of them are expected to be false positives. They found pairs in all mass ranges separated by 2000–47,000 AU at distances up to 4 kpc. Quinn & Smith (2009) searched for new wide halo binary stars in the SDSS Stripe 82 that satisfy CPM and photometric distance constraints. The projected separations of their pairs range from 0.007 to 0.25 pc. Longhitano & Binggeli (2010) used an "angular two-point correlation function" to do a purely statistical study of fragile binaries in a ∼675 deg^2 field centered at the North Galactic Pole using the DR6 stellar catalog. Their work predicted that there are more than 800 binaries with physical separations larger than 0.1 pc but smaller than 0.8 pc in this field. Dhital et al. (2010) presented a catalog of 1342 very wide (projected separation ⩾500 AU), low-mass (at least one mid-K to mid-M dwarf component) fragile pairs identified from astrometry, photometry, and proper motions in the SDSS Data Release Seven (DR7; Abazajian et al. 2009). In their catalog, 98.35% were expected to be physical pairs.

These previous fragile binary searches did not use spectral information such as radial velocity (RV) and metallicity. The SDSS provides medium-resolution spectra for about one million stars. We searched for fragile binary candidates using proper motion, RV, and metallicity information in the SDSS spectral archive catalog. RV and metallicity help to eliminate most random optical pairs.

Section 2 presents a discussion of our data selection method. The fragile binary candidates found are discussed in Section 3. Section 4 examines the chromospheric activity (CA) of the candidate pairs found and, for comparison, among SDSS stars in three open clusters. We conclude with a discussion of our findings in Section 5.

2. SAMPLE SELECTION

2.1. Overview of the SDSS Spectroscopic Data

The SDSS provides homogeneous and deep ($r < 22.5$) photometry in five bandpasses (u, g, r, i, and z; Gunn et al. 1998, 2006; Hogg et al. 2001; Smith et al. 2002; Tucker et al. 2006) accurate to ±0.02 mag (rms scatter) for unresolved sources not limited by photon statistics (Scranton et al. 2002). This sample has a zero-point uncertainty of ±0.02 mag (Ivezić et al.

2004). The SDSS also provides more than half a million stellar spectra with wavelength ranging from 3800 to 9000 Å. RV and metallicity are provided in the Table *sppParams* (Lee et al. 2008). Moreover, in Data Release Eight (DR8; Aihara et al. 2011a), all the stellar spectra obtained with the SDSS spectrograph were reprocessed through an improved stellar parameter pipeline, which improved the accuracy of metallicity estimates for stars up to solar metallicity. SDSS spectroscopy was carried out by twin fiber-fed spectrographs collecting 640 simultaneous observations. Typical exposure times were ∼15–20 minutes, but exposures were subsequently co-added for total exposure times of ∼45 minutes, producing medium-resolution spectra with $R \sim 2000$ (York et al. 2000). SDSS spectroscopic plates each contained 16 spectrophotometric standard stars, which were selected by color to be F subdwarf stars. The SDSS spectroscopic fluxes were calibrated by comparing these standard stars to a grid of theoretical spectra from model atmospheres (Kurucz 1993) and solving for a spectrophotometric solution for each plate.

2.2. Initial Data Selection

Our initial sample was selected mainly from three tables in DR8: *specphotoall*, *sppParams*, and *propermotions*.[3] The photometry and extinction values are provided in the Table *specphotoall*. The Table *sppParams* presented RV, $T_{\rm eff}$, log g, and [Fe/H], while the Table *propermotions* provided the proper motion of each star as matched with the U.S. Naval Observatory-B (USNO-B) survey (Munn et al. 2004). The original data can be accessed through CasJobs[4]. With the condition flag = “nnnnn” in Table *sppParams* and class = “star” in Table *specphotoall*, we obtained a first-cut sample containing 341,528 stars. Some stars with inaccurate photometry, extinction values, and illegal metallicity value (−99,999) were deleted, leaving 303,587 stars.

Aihara et al. (2011b) described some unexpected errors in the SDSS DR8 data that might cause a systematic shift in proper motion. To test the effect on our fragile binary candidates, we compared our sample’s proper motions in the DR7 and DR8 (see Figure 1). In right ascension, we found a systematic shift of 0.086 mas yr^{-1} with a scatter of about 3.4 mas yr^{-1}. In declination, there is a systematic shift of 0.096 mas yr^{-1} with a scatter of 2.8 mas yr^{-1}.

Our DR8 sample included 303,587 stars, but proper motions of only 219,844 of these stars can be found in DR7. We searched for fragile binary candidates among these 219,844 stars using the DR7 proper motions and found 53 candidates using our six constraints (see Section 3). Of these, 51 candidates are a subset of those found in the 303,587 star sample from DR8. Thus, the choice of DR7 or DR8 resulted in essentially the same candidate pairs common to both data sets. In order to start with a larger sample we chose to use the 303,587 stars having DR8 proper motion data.

3. FRAGILE BINARY CANDIDATE CATALOG

From the initial sample, we searched for fragile binaries using the following constraints.

1. Angular separation of $3'' < \theta < 250''$ between two nearby point sources A and B on the sky were selected, where θ was calculated from the small angle approximation:

$$\theta \simeq \sqrt{(\alpha_A - \alpha_B)^2 \cos\alpha_A \cos\alpha_B + (\delta_A - \delta_B)^2}. \quad (1)$$

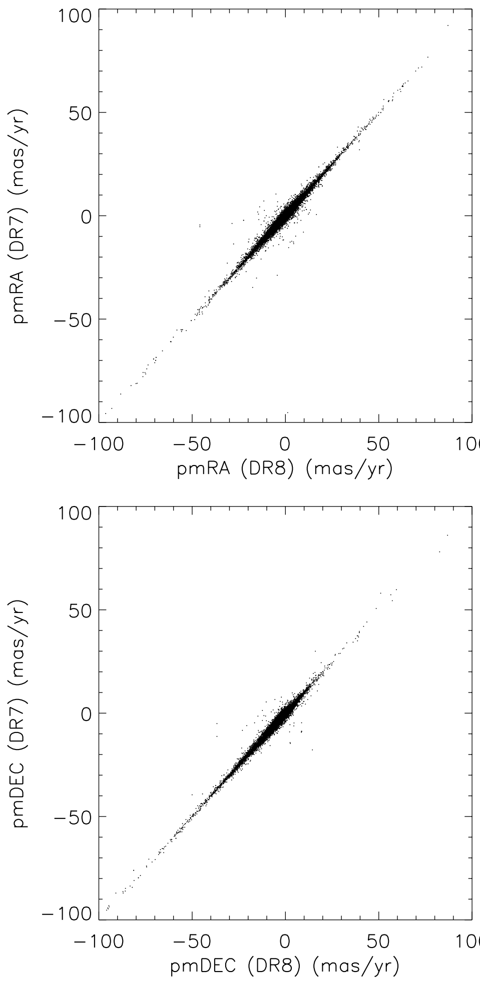

Figure 1. Comparison of the DR7 and DR8 proper motions. See the text for an explanation.

Sesar et al. (2008) constructed two independent samples of candidate fragile binaries: (1) $3'' < \theta < 16''$ and (2) $5'' < \theta < 30''$. Dhital et al. (2010) provided a fragile binary catalog with $7'' < \theta < 180''$. Although fragile binaries have been found at much larger angular separations (up to 900″ in Chanamé & Gould 2004, 1500″ in Lépine & Bongiorno 2007, and 570″ in Faherty et al. 2010), here we limited our maximum angular separation to 250″ since the number of random pairs with larger angular separations becomes unacceptably high in the deep SDSS survey. After this step, 68,414 pairs remained in our sample.

2. The maximum acceptable difference in proper motion, $\Delta|\mu| < 6$ mas yr^{-1}, was adopted where

$$\Delta|\mu| \equiv \sqrt{(\mu_{lA} - \mu_{lB})^2 + (\mu_{bA} - \mu_{bB})^2}. \quad (2)$$

The proper motions were queried from SDSS database in the Table ProperMotions which was derived by SDSS/USNO-B cross matching (Munn et al. 2004). We adopted the proper motions from the DR8 catalog which uses SDSS galaxies to recalibrate the USNO-B positions and SDSS stellar astrometry as an additional epoch for improved proper motion measurements. The typical 1σ error is ±3–4 mas yr^{-1} for each star. This is the reason we eliminated pairs with proper motion difference larger than 6 mas yr^{-1}. After this step, 22,964 pairs were left.

[3] http://www.sdss3.org/dr8/
[4] http://skyservice.pha.jhu.edu/casjobs/

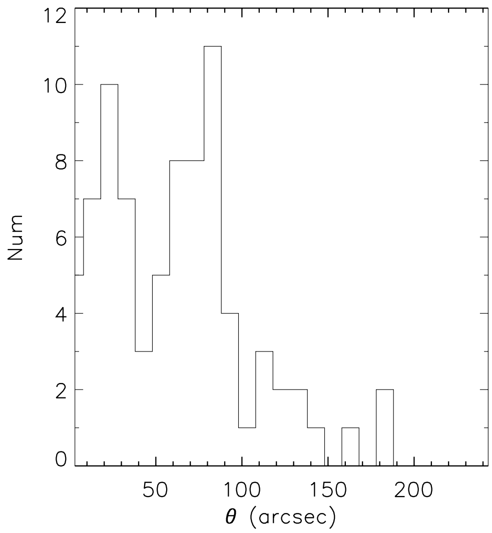

Figure 2. Angular separation θ distribution of our fragile binaries.

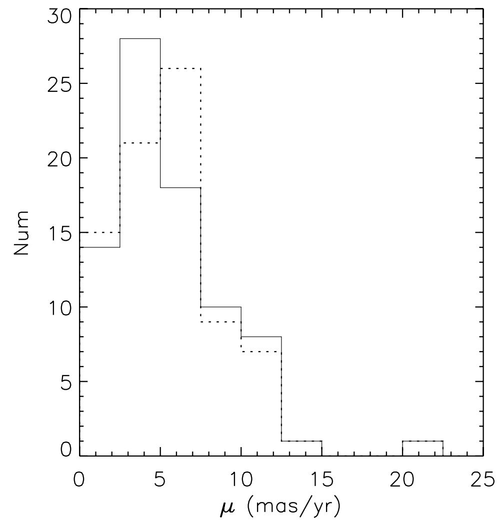

Figure 3. Proper motion distribution of the fragile binary candidates. The solid line represents primaries and the dashed line represents secondaries.

3. The constraint on RV we adopted for selection of a candidate pair was $|\Delta \mathrm{RV}| < 20$ km s^{-1}.

   The RV values are from the Table *sppParams*, which were measured by cross correlation with the ELODIE (Moultaka et al. 2004) stellar library. The typical error in RV is smaller than 10 km s^{-1}. Hence, we chose ΔRV smaller than 20 km s^{-1}. However, for higher RV stars, we only eliminated the pairs with ΔRV larger than 40 km s^{-1}. After this step, 6592 pairs remained.
4. We adopted an additional selection constraint based on metallicity, i.e., $|\Delta[\mathrm{Fe/H}]| < 0.3$.

   The metallicities are also from Table *sppParams* in the DR8 catalog. Several methods exist to estimate [Fe/H] (Lee et al. 2008). The typical error in [Fe/H] is no more than ±0.15 dex. Thus, pairs with $|\Delta[\mathrm{Fe/H}]| > 0.3$ were regarded as optical pairs. After this step, 3900 pairs remained.
5. We applied an additional candidate selection condition based on photometric distance, i.e., $\delta\, d < 40\%$.

   Physical pairs should have the same distances within the catalog uncertainties. Photometric parallax relations in the literature differ in the methodology used, photometric systems, and the absolute magnitude and metallicity range for which they are applicable. Not all of them are mutually consistent. Most exhibit intrinsic scatter of order ±0.5 mag or more. We adopted the relation from Ivezić et al. (2008), which gives the absolute magnitude in the r band, M_r as a function of color, $g - i$, and [Fe/H], as follows:

$$
\begin{aligned}
M_r = {} & -5.06 + 14.32(g-i) - 12.97(g-i)^2 \\
& + 6.127(\mathrm{g-i})^3 - 1.267(\mathrm{g-i})^4 + 0.0967(\mathrm{g-i})^5 \\
& + 4.5 - 1.1[\mathrm{Fe/H}] - 0.18[\mathrm{Fe/H}]^2.
\end{aligned}
\tag{3}
$$

   Since the typical uncertainty of photometric distance is more than 20%, we limited the selection of physical pair candidates to those with a computed distance difference smaller than 40%. After this step, 2260 pairs remained.
6. A selection criterion based on projected separation (a) was adopted, i.e., $a < 0.5$ pc. Pairs wider than this are believed to dissolve within the age of the Galaxy due to cumulative encounters with giant molecular clouds, distant encounters with other stars, and the Galaxy's tidal field (Weinberg et al. 1987). After this step, 80 candidate pairs remained in our final selected sample.

Table 1 lists the physical properties of these 80 pairs. Columns 1 and 2 list the α and δ; Columns 3–6 list the proper motions; RV and [Fe/H] are given in Columns 7–10; Columns 11–16 list the r magnitude, $g-i$ color, and spectral type, respectively. The last two columns list the angular separations in arcsec and projected separations in pc.

Figure 2 presents the angular separation (θ) distribution. It is bimodal with two peaks: $\theta = 25''$ and $\theta = 80''$. We made a statistical analysis of $g-r$, [Fe/H], and the dispersion of the W space motion (σ_{W}) for the primaries of the fragile pairs in each peak. The average $\langle g - r\rangle$ of these two peaks are 0.48 and 0.61; the average $\langle[\mathrm{Fe/H}]\rangle$ are −0.45 and −0.50; σ_{W} are 25 km s^{-1} and 22 km s^{-1}. Thus, there are no significant differences in metallicity and σ_{W} for these two peaks. Only the average $\langle g-r\rangle$ are a little different. Most primaries of fragile pairs in the first peak are G stars, while most primaries in the second peak are K stars. Although our maximum angular separation limit was $250''$, no pair was found with angular separation larger than $190''$.

Figure 3 shows the proper motion distribution. Since we did not set a low cutoff for proper motion, nearly 90% of our candidate pairs have proper motions lower than 13 mas yr^{-1}.

Figure 4 shows the reduced proper motion (RPM) diagram of the pairs, i.e., H_r versus $(g-r)_0$, where $H_r = r_0 + 5\log|\mu| + 5$. Equivalently, $H_r = M_r + 5*\log(V_{\mathrm{t}}) - 3.25$, where M_r is the absolute magnitude in the r band and V_{t} is the heliocentric tangential velocity in kilometers per second given by $V_{\mathrm{t}} = 4.74\, \mu d$. The dotted line indicates the division between the halo and disk, which was set by adopting $V_{\mathrm{t}} = 220$ km s^{-1} and $[\mathrm{Fe/H}] = -1.5$ and the photometric distance given by Ivezić et al. (2008). It is clear that our pairs are all disk stars.

Figure 5 shows the distance distribution of our pairs. All distances are larger than 100 pc. The peak at about 0.85 kpc indicates that our pairs are members of the disk. The thick solid line is an exponential fit:

$$N = 17.09 * \exp\left(\frac{-d}{0.81}\right) - 0.18. \tag{4}$$

Table 1
Properties of Fragile Binary Candidates

No.	SDSS Obj$_1$	SDSS Obj$_2$	pmα_1 (mas yr^{-1})	pmα_2 (mas yr^{-1})	pmδ_1 (mas yr^{-1})	pmδ_2 (mas yr^{-1})	RV$_1$ (km s^{-1})	RV$_2$ (km s^{-1})	[Fe/H]$_1$	[Fe/H]$_2$	r_1	r_2	$(g-i)_1$	$(g-i)_2$	(SP)$_1$	(SP)$_2$	$\Delta\theta$ ($''$)	a (pc)
1	J141918.7+002550	J141920.5+002535	−10	−9	−3	−8	−28	−32	−0.54	−0.78	16.79	18.11	0.70	0.97	F9	K1	31.03	0.349
2	J004839.6+151923	J004841.9+151818	3	6	−4	−5	−79	−96	−0.55	−0.32	14.34	17.23	0.69	1.78	F9	K7	73.59	0.269
3	J014701.4+150020	J014701.8+150014	−4	−7	−2	−4	−4	−6	−0.68	−0.76	16.37	18.27	0.60	1.16	G2	K3	8.41	0.088
4	J035711.1−070548	J035715.4−070604	4	7	4	7	4	−16	−0.74	−0.90	13.94	16.33	0.35	0.98	F5	K3	65.93	0.362
5	J100059.9−002450	J100100.4−002410	−9	−6	2	5	65	48	−0.32	−0.61	16.69	17.03	0.66	0.78	F9	F9	40.90	0.438
6	J094018.8+521326	J094010.1+521252	2	1	−7	−6	27	26	−0.36	−0.11	14.78	15.49	0.64	0.65	F9	F9	87.53	0.470
7	J234742.9−001205	J234741.3−001324	11	7	−5	−1	−1	16	−0.82	−0.72	16.11	16.57	0.72	1.31	F9	K5	83.22	0.405
8	J004830.1−000933	J004829.7−000917	11	15	−17	−17	15	18	−0.66	−0.93	16.64	17.76	1.29	1.89	K5	K7	16.99	0.072
9	J125817.5+590842	J125817.3+590907	−2	−4	−3	−2	3	3	−0.05	−0.24	14.76	16.63	0.65	1.27	F9	K5	25.34	0.153
10	J032230.9−004149	J032231.8−004141	3	1	−3	−1	6	−3	−0.22	−0.12	15.43	16.94	0.37	1.08	F5	K3	16.42	0.152
11	J031344.0+005201	J031342.9+005130	−1	0	−3	0	−21	−21	−0.45	−0.33	17.17	18.08	0.78	1.58	F9	K7	35.36	0.316
12	J074759.7+183505	J074800.5+183502	1	−4	0	−2	61	59	−0.51	−0.63	18.47	18.64	0.66	0.73	F9	F9	11.66	0.283
13	J003551.9+004254	J003550.1+004254	−2	−2	−10	−9	−26	−27	−0.39	−0.42	15.83	16.77	0.50	0.63	G2	F9	27.50	0.314
14	J203521.2+761923	J203515.4+761820	−5	−2	−9	−9	−41	−58	−0.50	−0.34	14.69	16.35	0.57	0.92	F9	K3	65.71	0.360
15	J033702.2−004010	J033709.8−004010	5	0	−8	−10	37	37	−0.25	−0.44	14.08	14.91	0.69	1.26	F9	K5	113.45	0.302
16	J221941.2+003400	J221939.4+003412	0	4	−5	−8	−59	−40	−0.58	−0.80	16.46	17.44	0.77	1.06	K1	K3	30.04	0.257
17	J221941.4−000353	J221938.5−000402	10	9	−11	−9	39	27	−0.51	−0.61	17.93	17.97	1.61	1.64	K5	K7	44.38	0.312
18	J221716.1−000346	J221717.6−000315	2	4	−3	−3	−20	−9	−0.23	0.02	15.40	15.81	0.81	0.92	K1	K1	37.82	0.217
19	J004731.1−004620	J004733.3−004607	1	2	−8	−5	−1	6	−0.75	−0.94	16.54	17.70	0.65	1.51	F9	K5	34.91	0.219
20	J031142.0−005018	J031142.3−005026	6	6	3	0	−23	−30	−0.69	−0.56	16.43	17.43	0.45	0.60	F2	F9	8.82	0.133
21	J025119.7−001345	J025121.7−001317	4	3	0	4	−9	−11	−0.19	−0.28	15.18	16.63	0.50	0.66	F9	F9	41.39	0.383
22	J005338.9+000230	J005340.3+000054	6	2	−5	−2	26	22	−0.36	−0.63	15.48	16.65	1.60	1.76	K7	K7	98.08	0.255
23	J030240.2+001000	J030239.3+000957	3	3	5	0	40	24	−0.62	−0.74	16.76	18.29	0.34	0.77	F5	K1	14.77	0.275
24	J012930.3+402816	J012922.6+402831	4	7	−7	−3	−2	0	−0.10	−0.36	14.64	15.42	0.86	0.98	K1	K1	88.79	0.362
25	J180746.3+243637	J180748.6+243525	−5	−7	−4	−8	−5	−9	−0.63	−0.45	15.19	16.27	0.63	0.82	F9	K1	78.24	0.457
26	J224438.4+230709	J224433.9+230653	−8	−6	−8	−8	−32	−33	−0.24	0.06	15.03	15.14	0.64	0.89	F9	K1	63.77	0.341
27	J020358.5−003207	J020401.8−003233	2	2	−1	−3	18	27	−0.77	−0.90	15.76	16.18	0.57	0.99	F2	K1	54.84	0.279
28	J173137.4+333408	J173136.1+333404	0	−2	−11	−10	41	48	−0.65	−0.83	16.22	18.00	0.56	0.92	F9	K1	16.80	0.181
29	J012439.9+402031	J012441.9+402013	−4	−3	−1	−5	−26	−28	−0.80	−0.78	15.37	17.20	0.30	0.55	F5	F9	29.22	0.425
30	J024416.0+004725	J024417.9+004719	1	−2	3	6	14	12	−0.24	−0.40	15.17	17.78	0.64	1.61	F9	K7	28.96	0.194
31	J024604.3+011348	J024601.7+011348	0	0	2	1	57	70	−0.78	−0.59	14.85	17.08	0.46	1.27	F5	K5	38.69	0.260
32	J040921.1−052701	J040927.0−052655	7	5	−3	1	58	53	−0.62	−0.46	15.02	16.80	0.76	1.59	F9	K7	89.43	0.390
33	J124144.1−014829	J124148.1−014952	−6	−7	6	9	5	7	−0.44	−0.40	14.31	15.67	0.67	0.97	F9	K3	102.22	0.404
34	J123925.0−023812	J123925.2−023739	−6	−2	−7	−5	46	50	−0.49	−0.58	14.47	16.02	0.69	1.39	F9	K5	32.59	0.122
35	J031737.1−072658	J031738.0−072533	1	2	4	8	33	31	−0.79	−0.91	16.21	16.28	0.95	0.95	K1	K1	86.36	0.476
36	J003044.2+142906	J003040.7+142921	3	4	3	0	2	−11	−0.06	−0.02	15.29	16.35	1.17	1.39	K5	K5	53.14	0.218
37	J095600.5+002626	J095601.4+002551	−5	0	−2	0	−8	−14	−0.40	−0.52	15.41	15.90	0.67	1.05	F9	K3	37.29	0.183
38	J170531.0+364758	J170535.9+364818	−4	−2	4	3	−33	−27	−0.20	−0.42	15.27	16.69	0.63	1.10	F9	K3	63.05	0.443
39	J082116.6+374008	J082122.1+374055	−4	0	−3	−2	−24	−31	−0.29	−0.25	16.04	16.95	1.12	1.44	K3	K5	80.74	0.438
40	J082923.4+394705	J082929.6+394635	1	−4	−3	−2	12	0	−0.62	−0.37	15.55	17.05	0.84	1.39	F9	K5	77.95	0.390
41	J082555.4+384633	J082602.0+384723	−3	−6	1	1	7	23	−0.74	−0.60	15.90	16.94	0.96	1.31	F9	K5	92.40	0.453
42	J081940.2+320117	J081939.3+320049	2	3	−1	4	70	50	−0.11	−0.37	16.98	17.28	1.28	1.34	K5	K5	31.34	0.238
43	J092513.8+442356	J092519.3+442251	−2	4	4	2	−20	−10	−0.36	−0.40	16.20	17.09	1.18	1.45	K3	K5	87.69	0.471
44	J075253.3+282215	J075250.4+282241	−3	−5	−6	−1	41	35	−0.37	−0.30	16.67	17.54	0.93	0.98	K1	K3	46.83	0.396
45	J141146.0+455747	J141152.8+455937	−1	0	−6	−4	0	−6	−0.13	−0.34	15.25	16.27	1.43	1.52	K5	K7	130.22	0.400
46	J131044.4+502744	J131039.9+502837	0	−4	−4	−4	−41	−38	−0.96	−0.66	15.67	17.09	0.77	1.49	F9	K5	68.52	0.350

Table 1
(Continued)

No.	SDSS Obj_1	SDSS Obj_2	$pm\alpha_1$ (mas yr^{-1})	$pm\alpha_2$ (mas yr^{-1})	$pm\delta_1$ (mas yr^{-1})	$pm\delta_2$ (mas yr^{-1})	RV_1 (km s^{-1})	RV_2 (km s^{-1})	$[Fe/H]_1$	$[Fe/H]_2$	r_1	r_2	$(g-i)_1$	$(g-i)_2$	$(SP)_1$	$(SP)_2$	$\Delta\theta$ ($''$)	a (pc)
47	J102043.7+094304	J102043.8+094151	0	−2	−5	−2	17	9	−0.62	−0.43	16.53	17.33	1.11	1.15	K3	K3	73.13	0.435
48	J103034.7+091759	J103034.3+091805	−3	−3	4	6	34	29	−0.42	−0.36	16.55	17.38	0.69	0.81	F9	F9	9.38	0.100
49	J100705.5+121349	J100701.7+121312	4	−1	7	6	46	44	−0.79	−0.89	16.37	17.40	0.94	1.33	K3	K5	67.13	0.410
50	J074435.9+175738	J074434.8+175727	−6	−3	−1	1	70	87	−0.59	−0.58	14.85	17.93	0.27	0.73	F5	F9	19.62	0.277
51	J130109.3+493750	J130115.9+493843	0	−3	3	0	−5	−14	−0.41	−0.15	15.74	16.15	1.32	1.68	K5	K7	82.99	0.297
52	J143126.9+081320	J143122.6+081311	−12	−9	1	0	−20	−3	−0.71	−0.81	16.35	16.54	0.63	0.93	F9	K3	66.15	0.436
53	J145450.7+105620	J145446.7+105714	−5	−1	−3	−7	3	0	−0.42	−0.14	15.63	16.12	1.18	1.38	K3	K5	80.14	0.323
54	J145257.7+325152	J145300.8+325112	6	3	−6	−4	−47	−46	−0.51	−0.68	17.03	17.55	0.91	1.23	K1	K5	56.22	0.467
55	J221556.6+682321	J221607.4+682039	4	7	−3	1	−48	−48	−0.28	−0.40	13.82	14.52	0.90	1.03	K3	K5	172.83	0.423
56	J221751.8+690949	J221726.7+690953	−1	0	−3	−5	−50	−65	−0.35	−0.22	14.12	14.80	0.73	0.76	K1	K1	133.97	0.457
57	J221428.5+682529	J221415.1+682619	0	2	2	1	−102	−115	−0.41	−0.31	14.29	14.80	0.74	0.86	K3	K3	89.31	0.313
58	J213425.9+730017	J213424.9+725850	−1	0	−4	0	−18	−3	−0.39	−0.34	14.01	14.40	0.74	0.84	K3	G5	87.19	0.275
59	J213410.2+734401	J213423.2+734547	4	1	2	6	−40	−38	−0.23	−0.43	14.69	15.05	0.84	0.93	K3	K3	119.35	0.465
60	J213206.3+750645	J213148.2+750553	−1	0	0	−4	−12	1	−0.07	−0.19	13.95	14.61	0.82	0.89	K1	K3	87.13	0.274
61	J010418.2+002633	J010422.3+002755	0	−1	−1	−2	−1	−6	−0.39	−0.39	15.59	16.59	1.01	1.38	K3	K5	102.77	0.478
62	J093741.6+291905	J093741.9+291737	−8	−6	3	0	7	9	−0.55	−0.60	14.31	16.11	0.45	1.20	G0	K3	88.21	0.402
63	J161348.9+505831	J161352.5+505729	−5	−2	5	6	−32	−13	−0.23	−0.15	15.78	17.25	1.14	1.61	K3	K7	70.69	0.342
64	J073427.2+652057	J073427.8+652037	1	0	1	−4	10	13	−0.44	−0.56	16.35	17.01	0.67	0.79	F9	F9	20.73	0.209
65	J080736.9+664653	J080725.3+664722	4	6	−3	1	−18	−14	−0.55	−0.60	15.71	16.38	0.78	0.91	F9	K1	74.64	0.452
66	J191817.1+365335	J191812.9+365322	5	4	0	−4	4	−15	−0.22	−0.45	15.67	18.47	0.68	1.37	F9	K5	52.02	0.414
67	J201548.9−130112	J201552.6−130114	−3	−2	−1	−1	−16	−18	−0.17	−0.20	16.85	16.95	1.42	1.63	K5	K7	53.68	0.288
68	J023335.5+264149	J023337.4+264204	−2	1	−1	0	−15	−12	−0.63	−0.53	16.24	17.32	0.50	0.90	G2	K1	29.05	0.317
69	J044715.1+214438	J044715.8+214254	2	3	−3	−4	24	24	−0.34	−0.45	13.84	14.64	0.75	0.76	K1	K1	104.24	0.305
70	J204024.3+561458	J204003.0+561354	−2	−3	−1	1	−48	−41	−0.03	−0.08	13.01	13.40	0.87	1.05	K3	K5	188.62	0.360
71	J204212.9+560534	J204228.2+560539	1	−2	3	1	−35	−51	−0.15	−0.00	12.89	13.51	0.84	0.94	K3	K5	127.29	0.232
72	J201647.3+595717	J201650.4+595717	−7	−6	2	−4	−36	−36	0.05	−0.09	14.44	16.20	0.66	1.39	F9	K5	23.16	0.117
73	J205345.0+573901	J205334.8+574102	−1	5	1	2	−24	−43	−0.35	−0.06	13.10	13.50	0.85	1.01	K3	K5	145.45	0.262
74	J192106.3+374460	J192058.8+374313	0	2	0	−2	−46	−45	0.46	0.27	13.59	13.70	1.19	1.23	K5	K5	139.18	0.308
75	J203959.7+564719	J203941.7+564526	−1	−2	1	7	−27	−10	−0.42	−0.40	13.19	13.77	0.75	0.87	K5	K5	186.16	0.386
76	J052006.9+172819	J052013.5+172714	3	2	1	1	25	19	−0.22	−0.42	14.32	14.89	0.84	0.86	K1	K1	114.11	0.388
77	J042405.9+070725	J042402.0+070717	9	5	−4	−6	1	1	−0.35	−0.49	15.20	15.22	0.66	0.72	K1	F9	59.47	0.321
78	J051613.4+165303	J051617.6+165145	−1	−1	−4	0	57	49	0.06	−0.03	14.65	14.67	0.73	0.91	K1	K1	98.20	0.397
79	J063503.6+275149	J063503.9+275139	0	0	2	2	51	36	−0.41	−0.68	16.74	17.35	0.42	0.47	G2	G0	11.50	0.251
80	J072816.6+145419	J072815.2+145414	−1	1	2	2	82	85	−0.42	−0.34	17.24	18.81	0.66	1.02	F9	K1	20.91	0.328

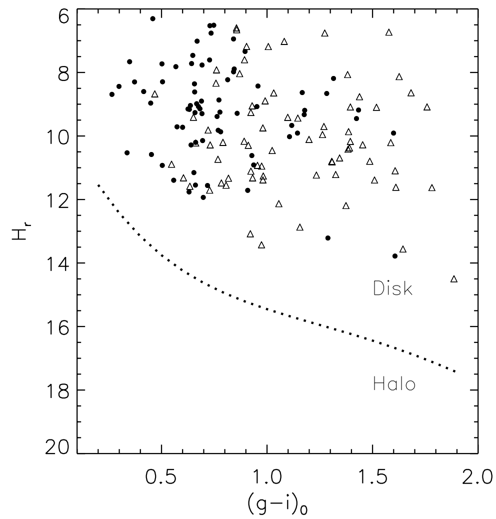

Figure 4. RPM of the fragile pairs. Filled circles and open triangles represent the (brighter) primaries and (fainter) secondaries of the pairs, respectively. The dotted line indicates the division between the halo and disk. The definition of this division line is illustrated in Section 3.

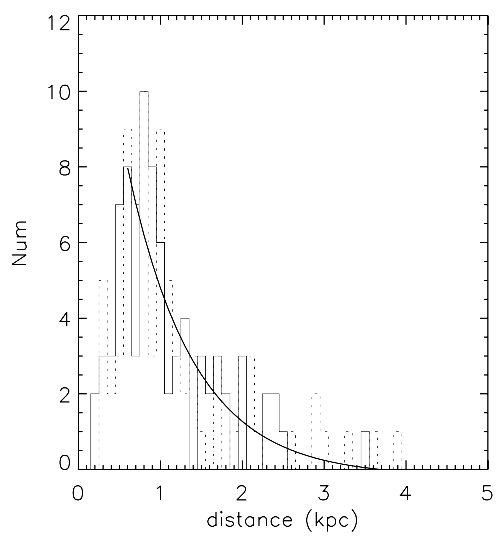

Figure 5. Distance distribution of fragile pairs. The solid line represents primaries and the dashed line represents secondaries. The thick solid line shows a fit with an exponential law of scale height 0.81 kpc.

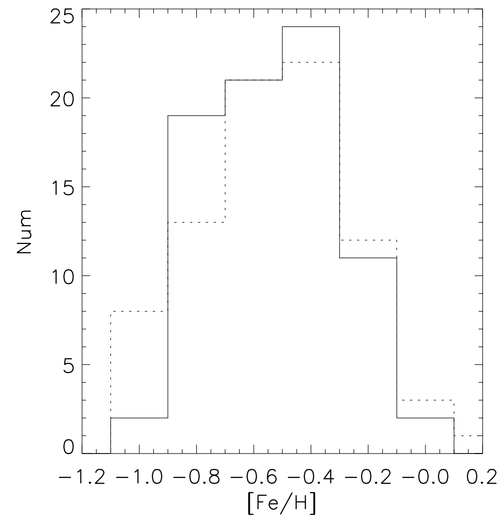

Figure 6. [Fe/H] distribution of our pairs. The solid line and the dashed line represent primaries and secondaries, respectively.

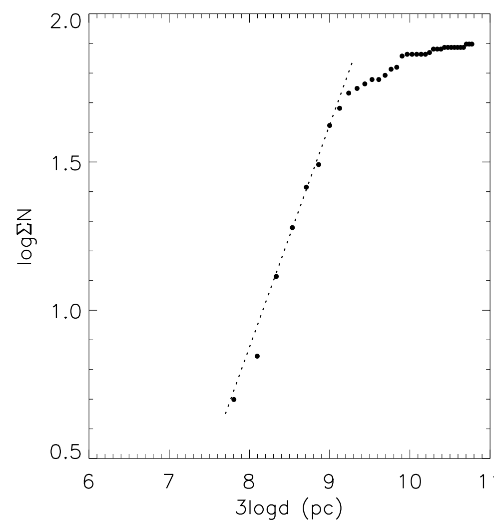

Figure 7. Completeness of our 80 candidate pairs. The distance d used for each binary candidate is the average of its two components' distance estimate. The straight line corresponds to $\Sigma N(d) \sim d^3$, i.e., a volume-complete sample.

Note that the scale height implied by this fit (0.81 kpc) is very similar to the generally accepted scale height of the Galaxy's thick disk (0.75 kpc; de Jong et al. 2010).

Figure 6 shows the metallicity [Fe/H] distribution of our pairs. A peak is evident at $[Fe/H] \sim -0.5$ dex, which provides more evidence that these pairs are disk stars.

Figure 7 shows a plot of $\log \Sigma N$ versus $3 \log d$, which tests the completeness of our sample. ΣN is the cumulative number of candidate pairs out to a distance d. The straight line corresponds to $\Sigma N \sim d^3$. As can be seen, the completeness is high only for pairs within about 1160 pc and falls off abruptly after that. This is primarily due to the projected separation limit set in our fragile binary search.

To investigate how the use of the spectroscopic sample in the SDSS influences their identification as possible wide binaries, we randomly selected 160 stars from the SDSS photometric sample. These 160 stars have no spectroscopic observations. Figure 8 shows a comparison between our sample which consists of 160 stars from the final 80 candidate pairs having spectra and the random photometric sample of 160 stars. The two samples almost have the same completeness in distance smaller than 1 kpc. At distances larger than 1 kpc, the photometric sample has better completeness than the spectroscopic sample, presumably because spectra are difficult to obtain in faint stars.

With the proper motion and photometric distance data, the rectangular velocity components relative to the Sun for these pairs were then computed and transformed into Galactic velocity components U, V, and W, and corrected for the peculiar solar motion $(U, V, W) = (-9, +12, +7)$ km s^{-1} (Wielen 1982). The UVW velocity components are defined as a right-handed system with U positive in the direction radially outward from the Galactic center, V positive in the direction of Galactic rotation, and W positive perpendicular to the plane of the Galaxy in the direction of the north Galactic pole. The uncertainties of the U, V, and W components were calculated based on the estimated errors in proper motion, distance, and RV using Equation (2) of Johnson & Soderblom (1987). Columns 2–7 in Table 2 list the U, V, and W velocity components and their uncertainties for each component in binary candidates. The U, V, and W differences

Table 2
Kinematical Properties of Fragile Binary Candidates

No.	U_1	V_1 (km s^{-1})	W_1	U_2	V_2 (km s^{-1})	W_2	Dist$_1$ (pc)	Dist$_2$ (pc)	ΔU	ΔV (km s^{-1})	ΔW	ΔDist (pc)	Age Consistency	Confidence
1	54 ± 42	-67 ± 48	2 ± 27	27 ± 58	-106 ± 67	-26 ± 40	1841	2147	27	39	28	306	NULL	E
2	-34 ± 12	-51 ± 11	58 ± 5	-33 ± 18	-72 ± 17	65 ± 8	598	789	1	21	7	191	Y	C
3	-44 ± 28	16 ± 32	-6 ± 19	-77 ± 42	18 ± 47	-28 ± 29	1711	1969	33	2	22	258	NULL	E
4	11 ± 17	7 ± 23	24 ± 16	8 ± 17	10 ± 23	49 ± 16	1056	899	3	3	25	157	Y	C
5	93 ± 45	-39 ± 28	1 ± 38	67 ± 38	-4 ± 26	25 ± 32	2065	1753	26	35	24	312	NULL	E
6	3 ± 10	-17 ± 15	37 ± 11	3 ± 15	-26 ± 23	38 ± 16	878	1333	0	9	1	455	NULL	B
7	30 ± 28	-42 ± 23	-19 ± 12	11 ± 16	0 ± 13	-14 ± 6	1165	796	19	42	5	369	Y	E
8	0 ± 25	-66 ± 25	-38 ± 8	8 ± 23	-54 ± 23	-33 ± 6	860	688	8	12	5	172	NULL	C
9	-8 ± 19	-8 ± 18	16 ± 9	0 ± 20	-10 ± 20	15 ± 9	988	1042	8	2	1	54	Y	A
10	-3 ± 33	-37 ± 46	7 ± 31	-10 ± 21	-1 ± 28	10 ± 18	2428	1511	7	36	3	917	NULL	E
11	-44 ± 30	-12 ± 40	2 ± 26	-27 ± 24	5 ± 31	19 ± 20	2010	1462	17	17	17	548	NULL	D
12	28 ± 51	-27 ± 84	51 ± 92	66 ± 51	-24 ± 83	-44 ± 92	4319	3973	38	3	95	346	NULL	E
13	-72 ± 37	-65 ± 39	-14 ± 16	-76 ± 43	-63 ± 44	-10 ± 18	1903	2154	4	2	4	251	Y	E
14	-63 ± 20	-16 ± 10	-6 ± 19	-72 ± 28	-23 ± 14	-28 ± 26	897	1214	9	7	22	317	NULL	D
15	13 ± 10	-24 ± 14	-19 ± 9	6 ± 7	-12 ± 9	-27 ± 5	611	435	7	12	8	176	Y	A
16	-7 ± 25	-55 ± 20	34 ± 18	-3 ± 32	-65 ± 26	-3 ± 25	1398	1448	4	10	37	50	NULL	D
17	-5 ± 34	-28 ± 26	-80 ± 25	0 ± 32	-24 ± 25	-62 ± 21	1224	1151	5	4	18	73	NULL	D
18	0 ± 17	-18 ± 12	9 ± 12	2 ± 20	-16 ± 15	-5 ± 16	940	1124	2	2	14	184	Y	A
19	-35 ± 31	-47 ± 33	-20 ± 11	-14 ± 21	-15 ± 22	-9 ± 5	1627	1026	21	32	11	601	NULL	E
20	30 ± 39	-14 ± 51	76 ± 33	11 ± 45	-53 ± 58	68 ± 38	2475	2904	19	39	8	429	NULL	E
21	1 ± 24	-16 ± 29	26 ± 18	21 ± 35	13 ± 44	47 ± 27	1515	2044	20	29	21	529	NULL	E
22	1 ± 9	0 ± 9	-20 ± 1	-2 ± 10	6 ± 10	-14 ± 2	426	544	3	6	6	118	Y	A
23	99 ± 71	30 ± 93	51 ± 60	29 ± 58	-26 ± 75	8 ± 48	4224	3043	70	56	43	1181	NULL	E
24	-3 ± 9	-13 ± 10	-11 ± 11	7 ± 11	-12 ± 11	2 ± 10	667	738	10	1	13	71	Y	A
25	-24 ± 13	-17 ± 14	16 ± 17	-45 ± 20	-43 ± 21	22 ± 26	955	1264	21	26	6	309	Y	E
26	-63 ± 20	-29 ± 13	14 ± 20	-48 ± 19	-31 ± 11	12 ± 16	1036	875	15	2	2	161	Y	A
27	6 ± 19	-5 ± 20	-7 ± 11	3 ± 14	-3 ± 15	-18 ± 7	1332	833	3	2	11	499	Y	A
28	-109 ± 32	-3 ± 27	10 ± 26	-122 ± 42	-11 ± 37	25 ± 37	1766	2120	13	8	15	354	NULL	E
29	-62 ± 31	11 ± 31	5 ± 29	-65 ± 38	-12 ± 40	-40 ± 42	2381	2693	3	23	45	312	NULL	E
30	8 ± 15	17 ± 19	5 ± 11	6 ± 21	36 ± 26	8 ± 14	1099	1194	2	19	3	95	NULL	D
31	29 ± 15	19 ± 19	-32 ± 10	34 ± 15	15 ± 19	-45 ± 11	1135	1098	5	4	13	37	NULL	B
32	36 ± 11	-30 ± 16	-17 ± 13	38 ± 12	-14 ± 17	-12 ± 13	713	758	2	16	5	45	Y	A
33	13 ± 15	8 ± 14	20 ± 6	28 ± 20	12 ± 19	28 ± 8	647	819	15	4	8	172	NULL	B
34	-13 ± 15	-40 ± 15	35 ± 7	-23 ± 13	-31 ± 12	42 ± 6	653	612	10	9	7	41	Y	A
35	21 ± 16	11 ± 19	-11 ± 10	33 ± 18	22 ± 21	0 ± 11	912	902	12	11	11	10	NULL	B
36	4 ± 13	7 ± 11	11 ± 7	0 ± 17	-9 ± 15	14 ± 8	671	913	4	16	3	242	Y	A
37	3 ± 20	0 ± 13	-17 ± 17	-15 ± 13	13 ± 9	-2 ± 11	1076	804	18	13	15	272	Y	C
38	29 ± 20	-20 ± 19	9 ± 18	17 ± 19	-11 ± 18	0 ± 16	1214	1151	12	9	9	63	Y	A
39	-19 ± 8	-3 ± 14	-23 ± 13	-34 ± 9	-3 ± 17	-12 ± 14	888	1036	15	0	11	148	Y	A
40	-2 ± 7	-6 ± 12	17 ± 10	1 ± 11	-2 ± 17	-9 ± 15	820	1067	3	4	26	247	Y	E
41	1 ± 7	9 ± 12	1 ± 11	24 ± 11	11 ± 16	-1 ± 16	802	993	23	2	2	191	Y	C
42	41 ± 12	-14 ± 21	51 ± 20	22 ± 13	15 ± 23	53 ± 21	1290	1240	19	29	2	50	NULL	E
43	-19 ± 9	19 ± 13	-12 ± 9	-30 ± 12	13 ± 15	13 ± 13	879	1014	11	6	25	135	Y	C
44	30 ± 12	-34 ± 27	0 ± 24	44 ± 20	0 ± 37	-25 ± 40	1382	2008	14	34	25	626	NULL	E
45	-18 ± 10	-5 ± 9	11 ± 4	-17 ± 12	-5 ± 11	5 ± 6	502	671	1	0	6	169	Y	A
46	-25 ± 15	-23 ± 15	-23 ± 6	-11 ± 19	-29 ± 19	-19 ± 7	835	883	14	6	4	48	Y	A
47	-10 ± 16	-22 ± 15	10 ± 12	0 ± 26	-11 ± 22	2 ± 19	974	1476	10	11	8	502	NULL	D
48	39 ± 32	9 ± 28	30 ± 22	53 ± 44	39 ± 40	36 ± 30	1749	2233	14	30	6	484	Y	E
49	7 ± 18	15 ± 16	63 ± 14	26 ± 20	8 ± 19	45 ± 16	999	1081	19	7	18	82	NULL	D
50	77 ± 24	-11 ± 37	-27 ± 45	85 ± 33	-4 ± 54	7 ± 61	2313	2903	8	7	34	590	NULL	E
51	-6 ± 11	10 ± 11	0 ± 4	-5 ± 11	-5 ± 11	-5 ± 3	614	584	1	15	5	30	Y	A
52	62 ± 33	-49 ± 37	25 ± 20	21 ± 21	-25 ± 24	21 ± 13	1579	1078	41	24	4	501	Y	E
53	-9 ± 11	-11 ± 13	13 ± 7	-22 ± 14	-17 ± 17	1 ± 9	659	784	13	6	12	125	Y	A
54	-58 ± 37	-10 ± 36	-53 ± 14	-31 ± 31	-14 ± 31	-42 ± 12	1564	1359	27	4	11	205	Y	E
55	-21 ± 8	-38 ± 4	-9 ± 8	-12 ± 9	-43 ± 4	-6 ± 9	400	454	9	5	3	54	NULL	B
56	-32 ± 10	-38 ± 5	-6 ± 10	-39 ± 13	-48 ± 6	-20 ± 15	558	774	7	10	14	216	NULL	B
57	-41 ± 10	-91 ± 5	-5 ± 10	-40 ± 12	-103 ± 6	-13 ± 12	574	650	1	12	8	76	NULL	B
58	-22 ± 9	-7 ± 4	-2 ± 10	-10 ± 9	2 ± 4	7 ± 9	516	542	12	9	9	26	NULL	B
59	-10 ± 13	-34 ± 5	-6 ± 13	-9 ± 13	-37 ± 6	7 ± 13	652	637	1	3	13	15	NULL	B
60	-16 ± 9	-5 ± 4	6 ± 9	-16 ± 11	11 ± 5	0 ± 11	515	605	0	16	6	90	N	E
61	-11 ± 12	2 ± 12	6 ± 4	-18 ± 15	1 ± 15	9 ± 5	761	866	7	1	3	105	Y	A
62	25 ± 15	13 ± 14	-11 ± 13	12 ± 10	2 ± 9	-1 ± 9	998	746	13	11	10	252	Y	A
63	16 ± 15	-22 ± 12	-5 ± 10	20 ± 22	0 ± 16	0 ± 14	792	1055	4	22	5	263	Y	C
64	-8 ± 20	13 ± 24	19 ± 19	16 ± 23	-21 ± 29	14 ± 21	1653	1759	24	34	5	106	Y	E
65	-24 ± 14	-20 ± 15	13 ± 13	-38 ± 16	-3 ± 16	25 ± 17	991	1117	14	17	12	126	NULL	D

Table 2
(Continued)

No.	U_1	V_1 (km s^{-1})	W_1	U_2	V_2 (km s^{-1})	W_2	Dist$_1$ (pc)	Dist$_2$ (pc)	ΔU	ΔV (km s^{-1})	ΔW	ΔDist (pc)	Age Consistency	Confidence
66	-2 ± 20	18 ± 11	-19 ± 24	-28 ± 46	-7 ± 22	-42 ± 49	1301	2014	26	25	23	713	NULL	E
67	-6 ± 12	-7 ± 13	26 ± 16	0 ± 10	-7 ± 12	18 ± 13	1040	879	6	0	8	161	NULL	B
68	-33 ± 22	2 ± 32	0 ± 27	-13 ± 20	-4 ± 30	17 ± 26	2049	1783	20	6	17	266	Y	C
69	13 ± 3	-1 ± 9	1 ± 8	13 ± 4	-7 ± 12	1 ± 11	478	645	0	6	0	167	NULL	B
70	-15 ± 5	-42 ± 2	0 ± 5	-13 ± 5	-35 ± 2	5 ± 5	322	312	2	7	5	10	NULL	B
71	-7 ± 5	-29 ± 2	3 ± 5	-13 ± 6	-45 ± 2	3 ± 6	298	381	6	16	0	83	Y	C
72	-19 ± 16	-35 ± 5	25 ± 17	-37 ± 17	-30 ± 5	9 ± 17	884	827	18	5	16	57	Y	C
73	-11 ± 5	-18 ± 2	6 ± 5	-5 ± 6	-37 ± 2	-2 ± 6	294	341	6	19	8	47	NULL	D
74	5 ± 5	-36 ± 2	-2 ± 6	3 ± 5	-36 ± 2	-5 ± 6	399	362	2	0	3	37	NULL	B
75	-11 ± 5	-21 ± 3	5 ± 6	-2 ± 7	-6 ± 3	15 ± 7	339	382	9	15	10	43	NULL	B
76	16 ± 3	0 ± 9	10 ± 9	10 ± 3	2 ± 11	10 ± 10	556	648	6	2	0	92	Y	A
77	-3 ± 11	-38 ± 22	26 ± 19	-11 ± 10	-29 ± 18	9 ± 15	1023	882	8	9	17	141	NULL	D
78	41 ± 4	-11 ± 15	-16 ± 14	37 ± 3	2 ± 10	-4 ± 10	870	661	4	13	12	209	NULL	B
79	41 ± 12	36 ± 63	29 ± 60	26 ± 13	31 ± 66	23 ± 64	3574	3642	15	5	6	68	Y	E
80	70 ± 23	-7 ± 40	29 ± 42	66 ± 38	-7 ± 65	56 ± 70	2566	3399	4	0	27	833	NULL	E

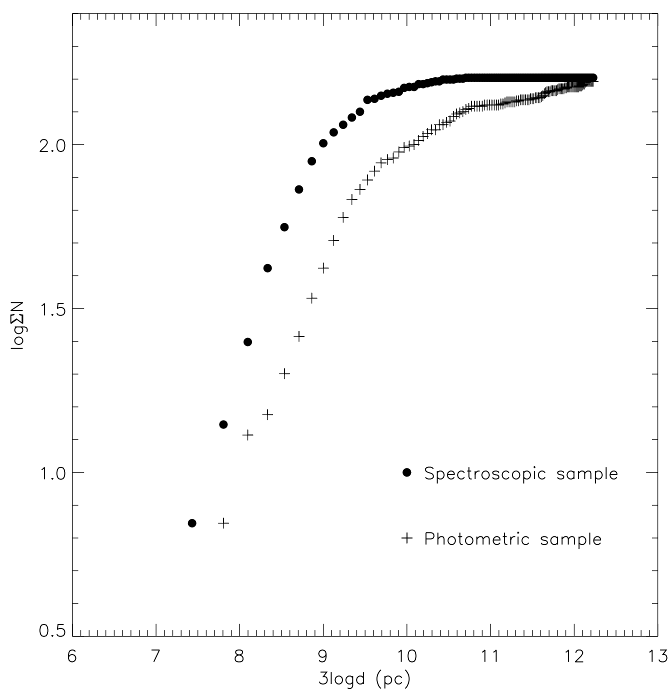

Figure 8. Completeness comparison between 160 stars in our final 80 fragile binary candidates (filled circles) and 160 stars randomly selected from the photometric sample (plus signs).

between two components of each pair are given in Columns 10–12.

The top panel of Figure 9 shows the U, V velocity contours, centered at $(U, V) = (0, -220)$ km s^{-1}, which represent 1σ and 2σ velocity ellipsoids for stars in the Galactic stellar halo as defined by Chiba & Beers (2000). The bottom panel of Figure 9 shows the Toomre diagram of candidate pairs (Venn et al. 2004). Stars with $V_{\rm total} > 180$ km s^{-1} are possible halo members. These plots indicate that all our pairs are disk stars.

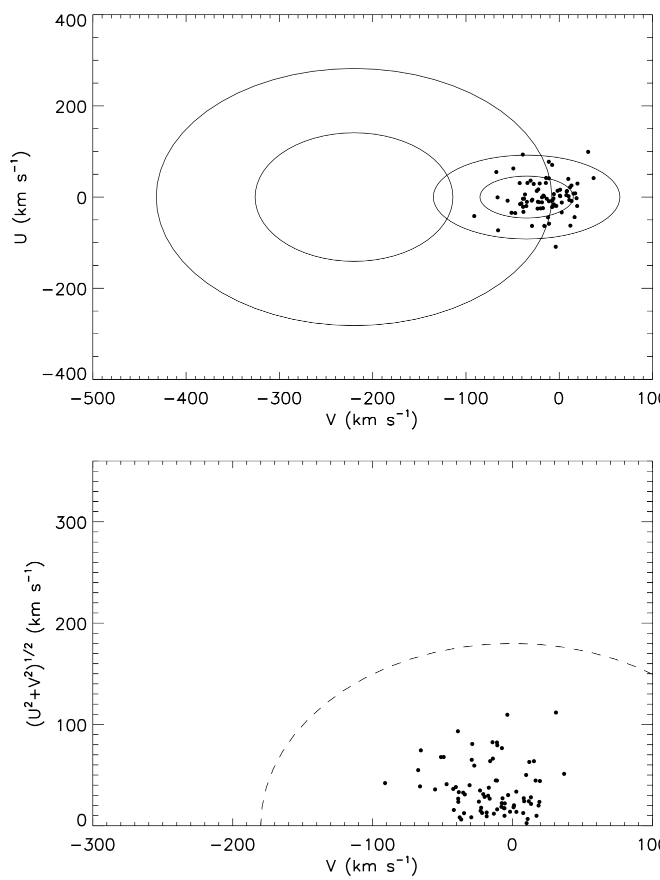

Figure 9. Top: UV–velocity distribution of our pairs. Ellipsoids indicate the 1σ (inner) and 2σ (outer) contours for Galactic thick disk and halo populations, respectively. Bottom: Toomre diagram of our pairs. The dashed line represents $V_{\rm total} = 180$ km s^{-1}.

4. CHROMOSPHERIC ACTIVITY MEASUREMENTS OF FRAGILE BINARY CANDIDATES

4.1. S_{HK} Measurement

For decades CA has been known to inversely correlate with stellar age (Skumanich 1972). Early work by Wilson (1963, 1968) and Vaughan & Preston (1980) established Ca II H and K emission as a useful marker of CA in stars. Following Hall et al. (2007), for each star we computed the flux ratio $S_{\rm HK}$:

$$S_{\rm HK} \equiv \alpha \frac{H + K}{R + V}, \quad (5)$$

where H and K are the fluxes measured in 2 Å rectangular windows centered on the line cores of Ca II H and K; R and V

are the fluxes measured in 20 Å rectangular "pseudocontinuum" windows on either side. These bands are essentially identical to those used in the Mount Wilson chromospheric activity survey program (Baliunas et al. 1995) except that the bands centered on Ca II *H* and *K* are wider (2 Å) than those used at Mount Wilson (1 Å) because of the resolution of SDSS spectra $R \sim 2000$. Here α is 10, representing the fact that the pseudocontinuum windows are 10 times wider than the *H* and *K* windows in wavelength coverage (Zhao et al. 2011).

Since there are 640 fibers in the SDSS spectrograph, there could be some systematic differences among spectra taken in different fibers. Stars with repeated observations provided the opportunity to measure the internal consistency of CA measurements. Eight stars with two or more spectroscopic observations were found. The mean $S_{\rm HK}$ difference between spectra for the same objects taken in different fibers is only about ± 0.002, thus we conclude that the fiber effect can be ignored in our CA analysis.

4.2. S_{HK} Measurements among MS Members of Open Clusters

In order to estimate the ages of fragile binary candidates, three open clusters, NGC 2420, M67, and NGC 6791, were selected for measurements of the $S_{\rm HK}$ from the SDSS DR8. The member stars of the three open clusters were selected based on the criteria from Smolinski et al. (2011). The age of NGC 2420 is about 2.0 Gyr (Von Hippel & Gilmore 2000), the age of M67 is about 4.05 Gyr (Jorgensen & Lindegren 2005), and the age of NGC 6791 is about 8 Gyr (Grundahl et al. 2008).

Figure 10 shows the color–magnitude diagrams (CMD) for these three clusters obtained from DR8 data. The top panel shows the CMD for NGC 2420, which has 138 dwarf stars. The CMD of this cluster is well defined. Unfortunately, most spectra of this cluster have signal to noise ratio (S/N) < 40. The middle panel shows the CMD for M67. It includes 72 member stars, all of which are dwarf stars whose spectra have S/N > 50. The bottom panel shows the CMD for NGC 6791, which is a very old open cluster. Forty-five member stars with good S/N were found in this cluster. Only two spectra have S/N < 40 (points indicated by squares in the bottom panel of Figure 10). In this cluster, high mass members have evolved off the main sequence (points indicated by plus sign in the bottom panel of Figure 10); these were omitted from the following analysis.

Figure 11 shows the $S_{\rm HK}$ versus $(g-r)_0$ diagram for these three open cluster member stars. Plus signs represent the member stars of M67, squares are member stars of NGC 2420, and triangles represent the member stars of NGC 6791. The dotted lines represent the least-squares fitted lines for NGC 2420 with $\pm 1\sigma$, the dashed lines the fitting for M67, while the dashed-dot lines represent the fitting for NGC 6791. All the fitted lines are parabolas. The scatter in NGC 2420 is large because the S/N of the spectra is very low. The NGC 6791 fitted line is concave down only because this evolved cluster has no blue stars on the upper main sequence to define the curvature.

4.3. The Age Estimation of Fragile Binary Candidates

Although the scatter of $S_{\rm HK}$ is appreciable within each cluster (especially in NGC 2420 and NGC 6791), the mean relations in Figure 11 clearly show that $S_{\rm HK}$ declines with age. NGC 2420 has stronger CA at each $(g-r)_0$ color than the other two clusters, indicating that it is the youngest cluster.

Figure 12 displays $S_{\rm HK}$ versus $(g-r)_0$ for the 38 fragile binaries with S/N > 40. In this figure, the mean

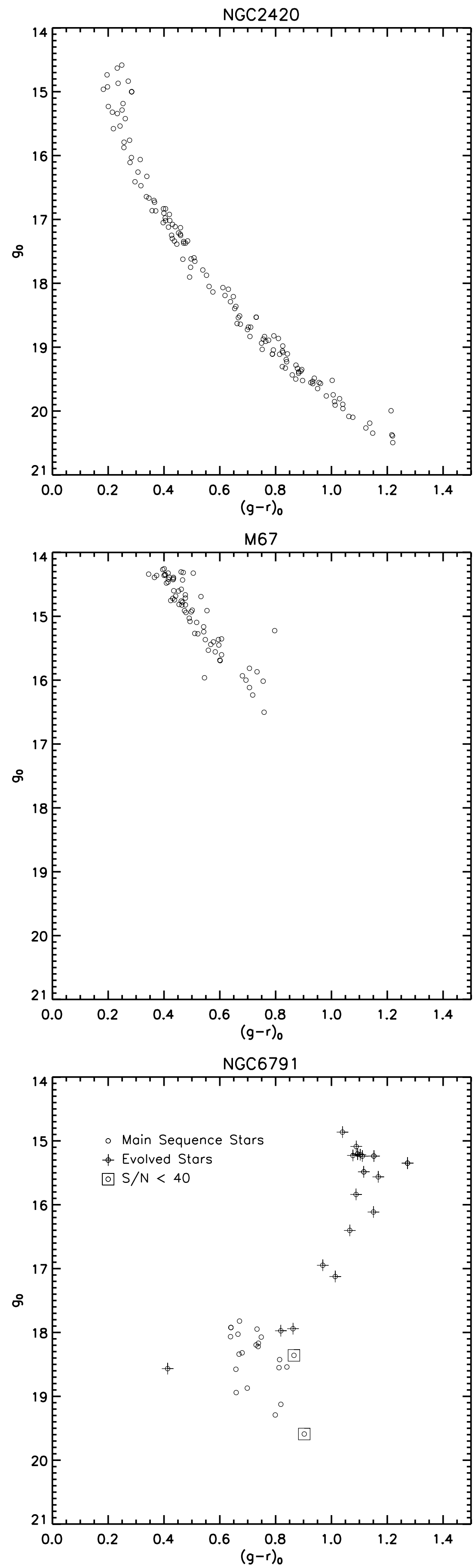

Figure 10. CMD diagrams of NGC 2420, M67, and NGC 6791.

Table 3
Criteria of Confidence Levels of Being Physical Pairs

Level	UVW Differences (km s^{-1})	UVW Uncertainties (km s^{-1})	Distance Differences (pc)	Age Consistency
"A"	<15	<20	<500	Y
"B"	<15	<20	<500	NULL
"C"	<35	<35	<500	Y
"D"	<35	<35	<500	NULL

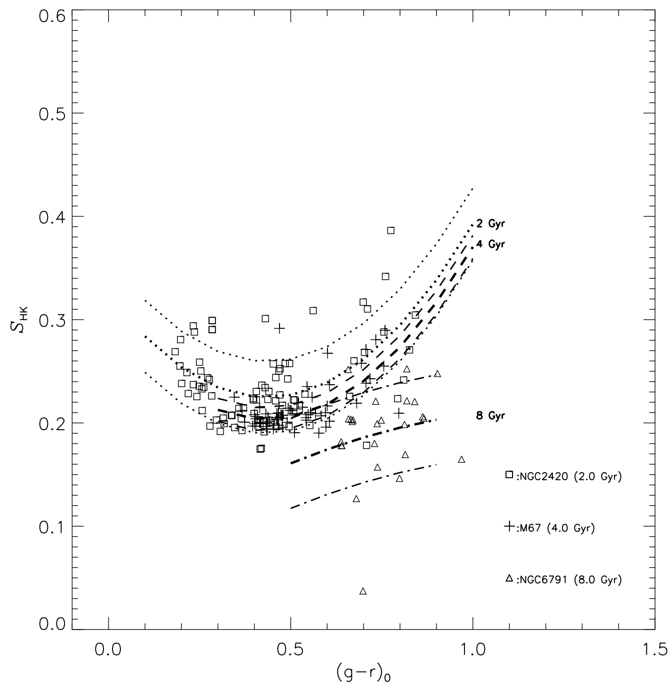

Figure 11. S_{HK} vs. $(g-r)_0$ for three open clusters. Plus signs represent member stars of M67, squares are stars of NGC 2420, while triangles indicate the member stars of NGC 6791. The thick dotted lines represent the least-squares fitting for NGC 2420 and $\pm 1\sigma$, the dashed lines for M67, and the dashed-dot lines for NGC 6791.

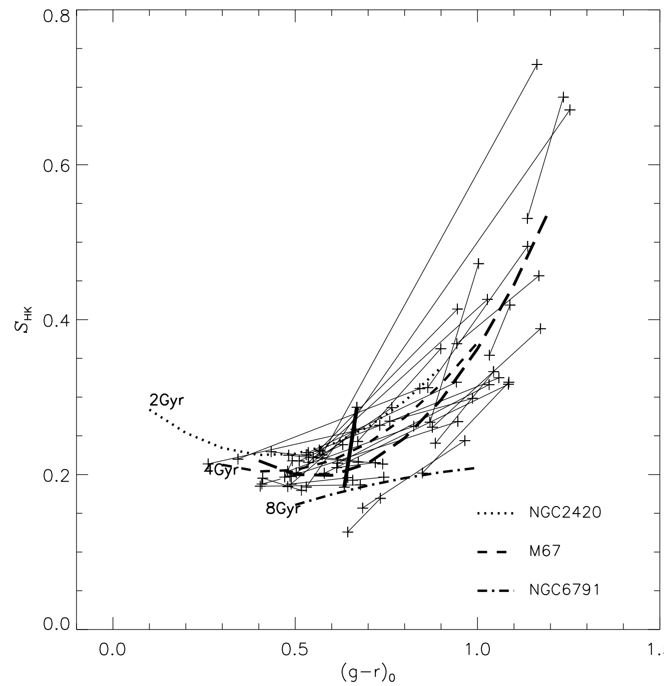

Figure 12. S_{HK} vs. $(g-r)_0$ for fragile binary candidates. Solid lines connect two components of each pair. The dashed line is the distribution of M67 (4.0 Gyr); the dotted line represents the least-squares fitting for NGC 2420 (2.0 Gyr) while the dashed-dot line for NGC 6791 (8.0 Gyr). Thick solid line connects the pair which is not a physical pair with high probability. The long dashed line shows the least-squares fitting for all fragile candidates.

relation for the three clusters in Figure 11 is overplotted. The fitting lines of these three clusters can be used to roughly gauge the ages of our fragile pairs. Evidently, the age of the two lowest pairs (J204212.9+560534 and J204228.2+560539; J082555.4+384633 and J082602.0+384723) is about the same as NGC 6791, i.e., 8 Gyr. The semimajor axes of these two pairs are 0.4 pc and 0.2 pc. Most pairs have about the same age as M67. Nearly all the pairs' components have consistent CA level for their $(g-r)_0$ color, indicating that they are indeed coeval. Only one pair, SDSS J213206.3+750645 and SDSS J213148.24+750552.63 (connected by a thick solid line in Figure 12), appears to be nonphysical. Column 15 in Table 2 presents the age consistency of these 38 pairs. "Y" indicates that two components have consistent ages, "N" indicates inconsistent ages, and "NULL" indicates stars that are not part of the sample of these 38 candidates.

A long dashed line shows the least-squares fitting for all the 80 candidate pairs. It lies mostly between 4 Gyr and 8 Gyr. If we suppose there is a linear relation between age and S_{HK} at each $(g-r)_0$, the mean age of these pairs is about 5 Gyr, i.e., about the same as the Sun.

For each binary candidate, we adopted a rough confidence level for being a physical pair. We set five levels: "A," "B," "C," "D," and "E." The criteria for level "A," "B," "C," and "D" are shown in Table 3. Candidate pairs that do not satisfy criteria "A" to "D" are given level "E." Level "A" means that candidate is very likely to be a physical pair, while "E" corresponds to the lowest probability.

5. CONCLUSIONS

We found 80 fragile binary candidates with low proper motion based on CPM, RV, metallicity, and photometric distance. All these pairs have very large projected separations. They are all disk stars based on our analysis of their space motions, metallicities, and RPM. The S/N of the spectra for half of these pairs are high enough to measure the CA index S_{HK}. Measurements of S_{HK} for stars in three open clusters allowed us to make a very preliminary estimate of the age of these pairs. The mean age of these fragile candidate pairs is about 5 Gyr. Our results suggest that at least some fragile pairs ($a \sim 0.4$ pc) can survive 8 Gyr in the Galactic disk. Additional more accurate observations are needed to confirm the truly physical pairs among these candidates.

We are grateful for constructive comments by the referee that substantially improved our paper. T.D.O. acknowledges support from NSF grant AST-0807919 to the Florida Institute of

Technology. J.K.Z. and G.Z. acknowledge support from NSFC grant Nos. 10821061 and 11078019.

Funding for SDSS-III has been provided by the Alfred P. Sloan Foundation, the Participating Institutions, the National Science Foundation, and the U.S. Department of Energy Office of Science. The SDSS-III Web site is http://www.sdss3.org/.

SDSS-III is managed by the Astrophysical Research Consortium for the Participating Institutions of the SDSS-III Collaboration including the University of Arizona, the Brazilian Participation Group, Brookhaven National Laboratory, University of Cambridge, University of Florida, the French Participation Group, the German Participation Group, the Instituto de Astrofisica de Canarias, the Michigan State/Notre Dame/JINA Participation Group, Johns Hopkins University, Lawrence Berkeley National Laboratory, Max Planck Institute for Astrophysics, New Mexico State University, New York University, Ohio State University, Pennsylvania State University, University of Portsmouth, Princeton University, the Spanish Participation Group, University of Tokyo, University of Utah, Vanderbilt University, University of Virginia, University of Washington, and Yale University.

REFERENCES

Abazajian, K. N., Adelman-McCarthy, J. K., Agüeros, M. A., et al. 2009, ApJS, 182, 543
Adelman-McCarthy, J. K., Agüeros, M. A., Allam, S. S., et al. 2008, ApJS, 175, 297
Aihara, H., Allende Prieto, C., An, D., et al. 2011a, ApJS, 193, 29
Aihara, H., Allende Prieto, C., An, D., et al. 2011b, ApJS, 195, 26
Baliunas, S. L., Donahue, R. A., Soon, W. H., et al. 1995, ApJ, 438, 269
Chanamé, J., & Gould, A. 2004, ApJ, 601, 289
Chanamé, J. 2007, in IAU Symp. 240, Binary Stars as Critical Tools & Tests in Contemporary Astrophysics, ed. W. I. Hartkopf, E. F. Guinan, & P. Harmanec (Cambridge: Cambridge Univ. Press), 316
Chiba, M., & Beers, T. C. 2000, AJ, 119, 2843
Cutri, R. M., Skrutskie, M. F., van Dyk, S., et al. 2003, 2MASS All Sky Catalog of Point Sources (The IRSA 2MASS All-Sky Point Catalog, NASA/IPAC Infrared Science Archive, http://irsa.ipac.caltech.edu/applications/Gator/)
de Jong, J. T. A., Yanny, B., Rix, H., et al. 2010, ApJ, 714, 663
Dhital, S., West, A. A., Stassun, K. G., & Bochanski, J. J. 2010, AJ, 139, 2566
Faherty, J. K., Burgasser, A. J., West, A. A., et al. 2010, AJ, 139, 176
Greenstein, J. L. 1986, AJ, 92, 859
Grundahl, F., Clausen, J. V., Hardis, S., & Frandsen, S. 2008, A&A, 492, 171
Gunn, J. E., Carr, M., Rockosi, C., et al. 1998, AJ, 116, 3040
Gunn, J. E., Siegmund, W. A., Mannery, E. J., et al. 2006, AJ, 131, 2332
Halbwachs, J. L. 1986, A&AS, 66, 131
Hall, J. C., Lockwood, G. W., & Skiff, B. A. 2007, AJ, 133, 862
Hogg, D. W., Finkbeiner, D. P., Schlegel, D. J., & Gunn, J. E. 2001, AJ, 122, 2129
Ivezić, Z., Lupton, R. H., Schlegel, D., et al. 2004, Astron. Nachr., 325, 583
Ivezić, Z., Sesar, B., Jurić, M., et al. 2008, ApJ, 684, 287
Jiang, Y. F., & Tremaine, S. 2010, MNRAS, 401, 977
Johnson, D. R., & Soderblom, D. R. 1987, AJ, 93, 4
Jorgensen, B. R., & Lindegren, L. 2005, A&A, 436, 127
Kouwenhoven, M. B. N., Goodwin, S. P., Parker, R. J., et al. 2010, MNRAS, 404, 1835
Kurucz, R. L. 1993, Kurucz CD-ROM 13, ATLAS9 Stellar Atmosphere Programs and 2 km/s Grid (Cambridge: SAO)
Lawrence, A., Warren, S. J., Almaini, O., et al. 2007, MNRAS, 379, 1599
Lee, Y. S., Beers, T. C., Sivarani, T., et al. 2008, AJ, 136, 2022
Lépine, S., & Bongiorno, B. 2007, AJ, 133, 889
Lépine, S., & Shara, M. M. 2005, AJ, 129, 1483
Longhitano, M., & Binggeli, B. 2010, A&A, 509, A46
Luyten, W. J. 1979, Proper Motion Survey with the 48 Inch Telescope (Minneapolis, MN: Univ. Minnesota Press)
Luyten, W. J. 1988, Ap&SS, 142, 17L
Moultaka, J., Ilovaisky, S. A., Prugniel, P., & Soubiran, C. 2004, PASP, 116, 693
Munn, J. A., Monet, D. G., Levine, S. E., et al. 2004, AJ, 127, 3034
Quinn, D. O., & Smith, M. C. 2009, MNRAS, 400, 2128
Salim, S., & Gould, A. 2003, ApJ, 582, 1011
Scranton, R., Johnston, D., Dodelson, S., et al. 2002, ApJ, 579, 48
Sesar, B., Ivezić, Z., & Jurić, M. 2008, ApJ, 689, 1244
Skumanich, A. 1972, ApJ, 171, 565
Smith, J. A., Tucker, D. L., Kent, S., et al. 2002, AJ, 123, 2121
Smolinski, J. P., Lee, Y. S., Beers, T. C., et al. 2011, AJ, 141, 89
Tucker, D., Kent, S., Richmond, M. W., et al. 2006, Astron. Nachr., 327, 821
Vaughan, A. H., & Preston, G. W. 1980, PASP, 92, 385
Venn, K. A., Irwin, M., Shetrone, M. D., et al. 2004, AJ, 128, 1177
Von Hippel, T., & Gilmore, G. 2000, AJ, 120, 1384
Weinberg, M. D., Shapiro, S. L., & Wasserman, I. 1987, ApJ, 312, 367
Wielen, R. 1982, Landolt-Börnstein Tables, Astrophysics, Vol. 2C, Section 8.4 (Berlin: Springer), 202
Wilson, O. C. 1963, ApJ, 138, 832
Wilson, O. C. 1968, ApJ, 153, 221
York, D. G., Adelman, J., Anderson, J. E., Jr., et al. 2000, AJ, 120, 1579
Zhao, J. K., Oswalt, T. D., Rudkin, M., Zhao, G., & Chen, Y. Q. 2011, AJ, 141, 107